Porous Carbon Nano-sheets as Excellent Carbocatalysts for Organic Pollutants Removal via Persulfate Activation: The Role of sp^2/sp^3 Carbon Ratio

Qi Fu[a], Huangsheng Yang[a], Jiaxing Yu[a], Li Nan[a], Yuanjun Tong[a], Songbo Wei[a], Zhengping Hao[b], Junhui Wang[a, *], Gangfeng Ouyang[a,c,d]

[a] MOE Key Laboratory of Bioinorganic and Synthetic Chemistry/KLGHEI of Environment and Energy Chemistry, School of Chemistry, Sun Yat-Sen University, Guangzhou, Guangdong, 510275, China

[b] National Engineering Laboratory for VOCs Pollution Control Material & Technology, University of Chinese Academy of Sciences, Beijing 101408, China

[c] College of Chemistry & Molecular Engineering, Center of Advanced Analysis and Computational Science, Zhengzhou University, Zhengzhou 450001, China

[d] Guangdong Provincial Key Laboratory of Emergency Test for Dangerous Chemicals, Guangdong Institute of Analysis (China National Analytical Center Guangzhou), Guangdong Academy of Science ,100 Xianlie Middle Road, Guangzhou 510070, China

---

* Corresponding author:

Tel: +86 020 84110845/0953; fax: +86 020 84110845/0953.

E-mail address: wangjh36@mail.sysu.edu.cn (J. Wang).

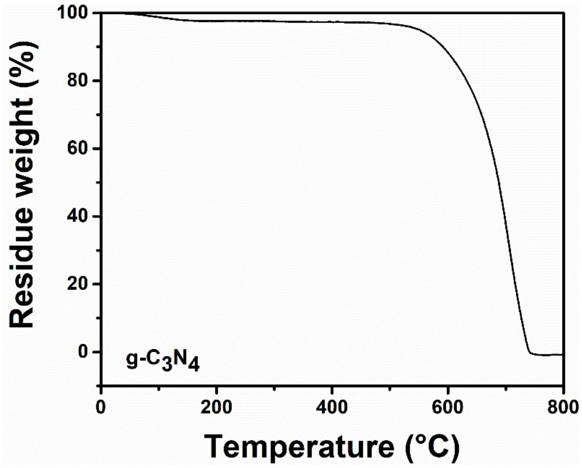

Fig. S1 TGA of g-C_3N_4 in N_2 with a temperature rise rate of 10 °C min^{-1}.

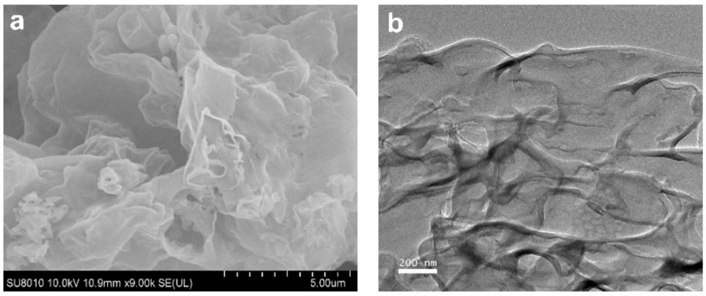

Fig. S2 (a) SEM image of pristine g-C_3N_4. (b) TEM image of pristine g-C_3N_4.

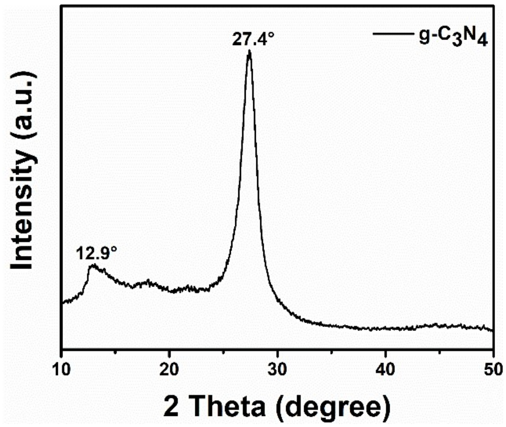

Fig. S3 XRD pattern of g-C_3N_4.

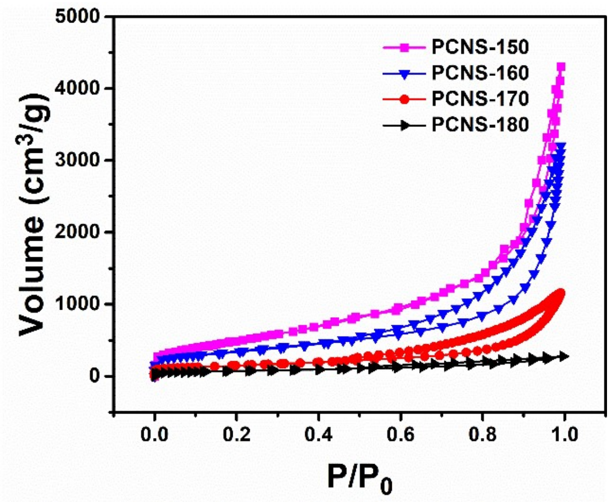

Fig. S4 N_2 adsorption/desorption isotherms.

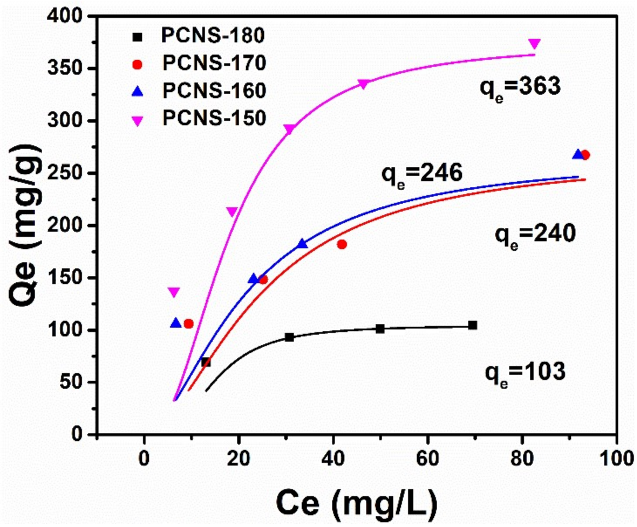

Fig. S5 The fitting curves of Langmuir model for the adsorption isotherms of BPA on the PCNSs.

Ce (mg L^{-1}) is the concentration of equilibrium adsorption in the solution, and Qe (mg g^{-1}) is the equilibrium adsorption capacity.

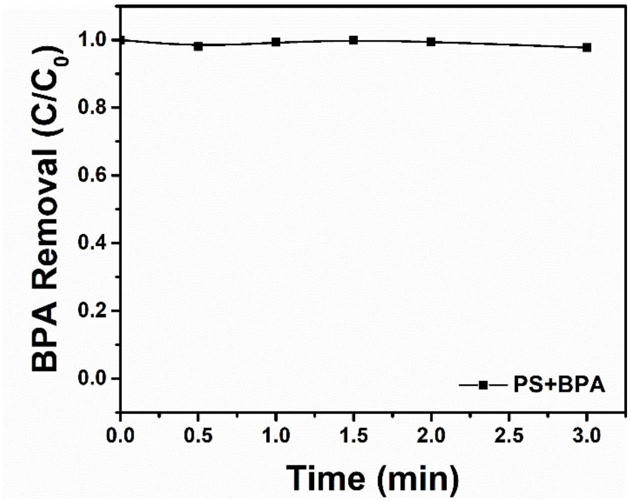

Fig. S6 Degradation curve of BPA in the presence of PS. [PS] = 1.5 mM; [BPA] = 80 mg/L.

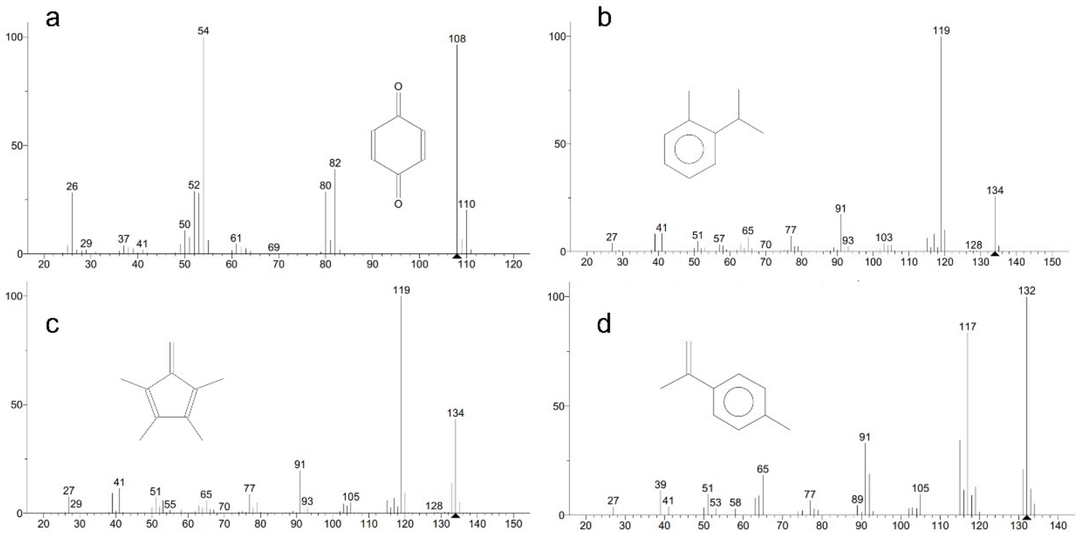

Fig. S7 GC-MS spectra of the BPA degradation intermediates.

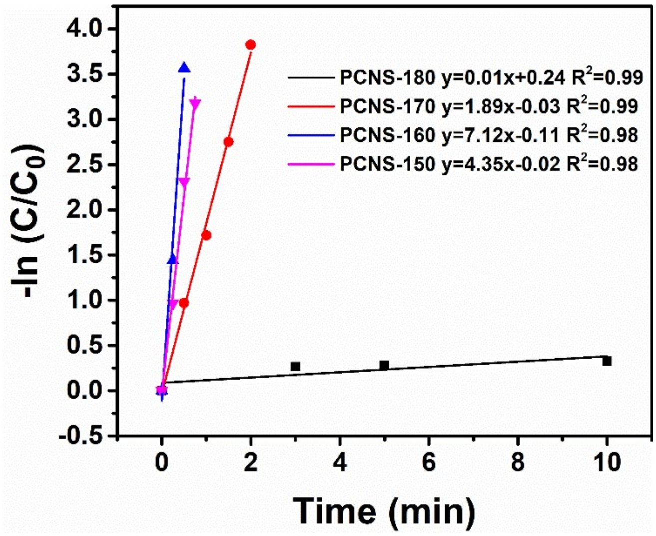

Fig. S8 The kinetic analyses of BPA degradation to pseudo-first-order model.

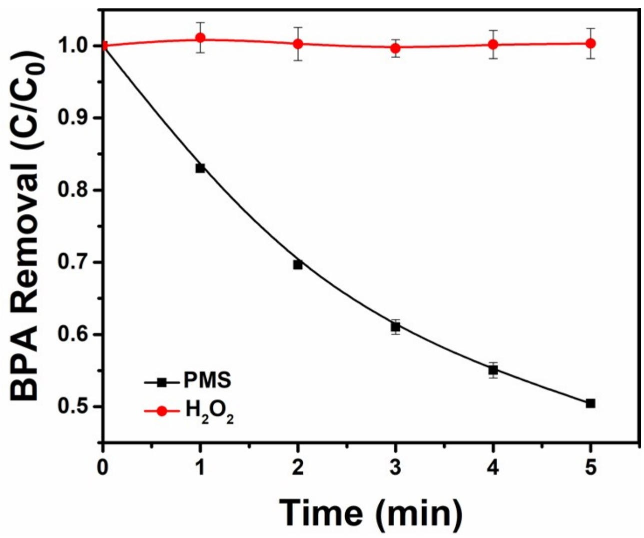

Fig. S9 The effects of different oxidants on BPA degradation [PCNS] = 0.1 g/L; [PMS] = [H_2O_2] = 1.5 mM; [BPA] = 80 mg/L.

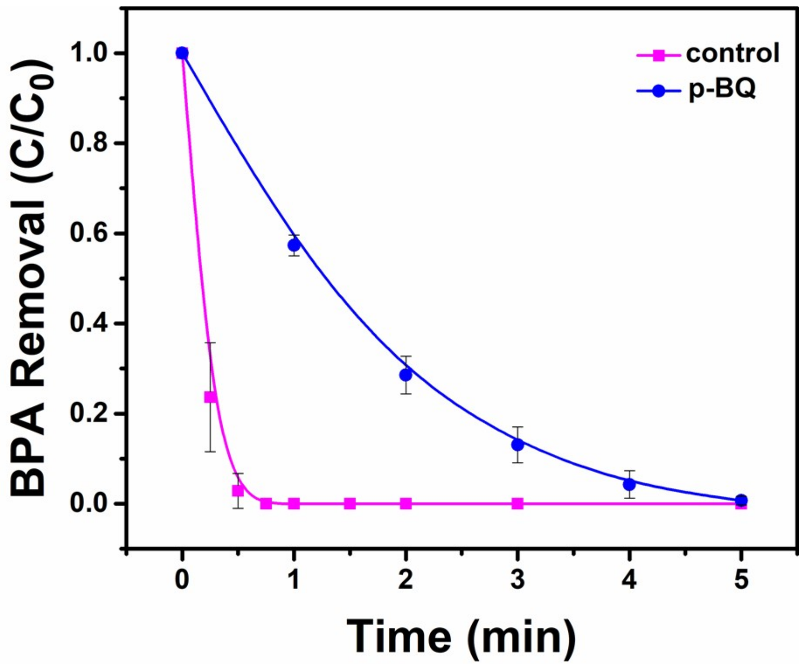

Fig. S10 The effects of p-BQ on BPA degradation [PCNS-160] = 0.1 g/L; [PS] = 1.5 mM; [p-BQ] = 7.5 mM [BPA] = 80 mg/L.

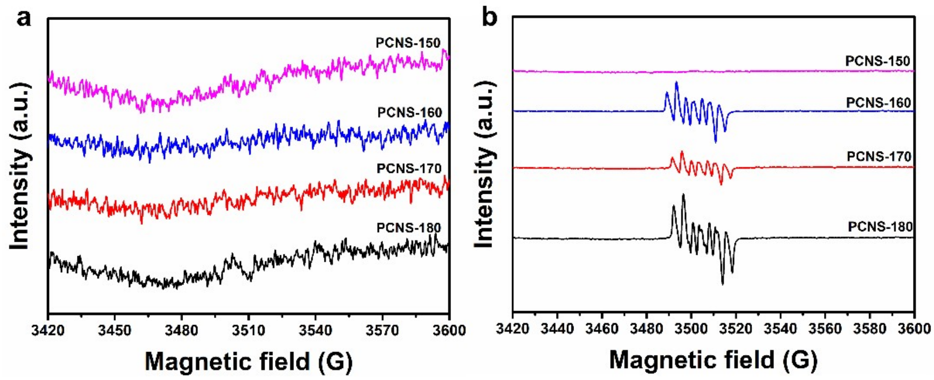

Fig. S11 EPR spectra obtained by spin trapping with TEMP and DMPO in the presence of PS and PCNSs. [PCNS] = 0.1 g/L; [PS] = 1.5 mM; [BPA] = 80 mg/L; [DMPO/TEMP] = 10 mM.

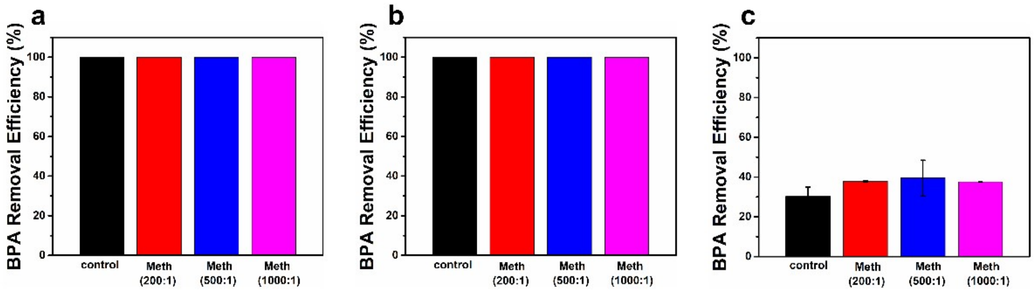

Fig. S12 Effects of methanol on BPA removal in (a)PCNS-150/PS system, (b) PCNS-170/PS system and (c) PCNS-180/PS system. [PCNS] = 0.1 g/L; [PS] = 1.5 mM; [BPA] = 80 mg/L.

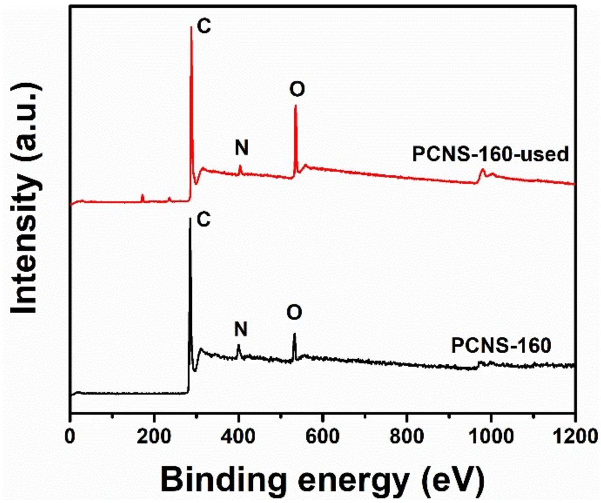

Fig. S13 XPS survey of PCNS-160 and PCNS-160-used.

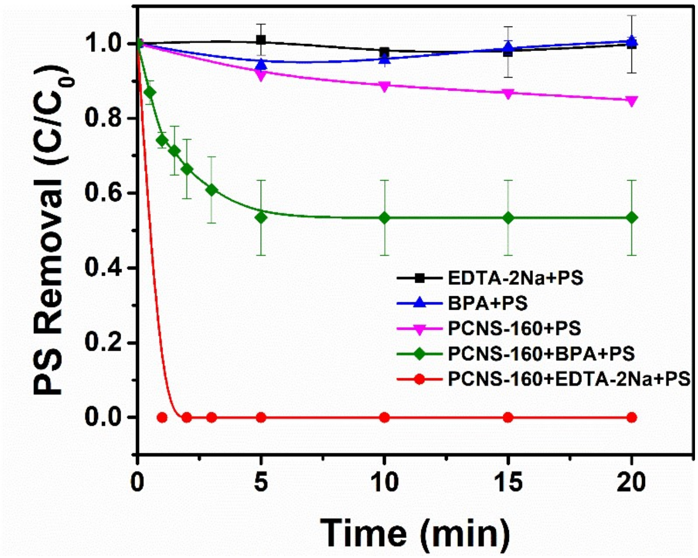

Fig. S14 Consumption curves of PS. [PS] = 1.5 mM; [PCNS-160] = 0.1 g/L; [BPA/EDTA-2Na] = 0.36 mM.

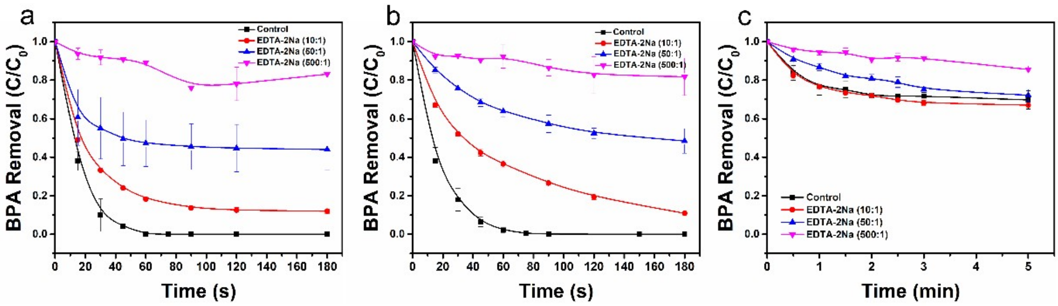

Fig. S15 Effects of EDTA-2Na on BPA removal in (a)PCNS-150/PS system, (b) PCNS-170/PS system, (c) PCNS-180/PS system. [PCNS] = 0.1 g/L; [PS] = 1.5 mM; [BPA] = 80 mg/L.

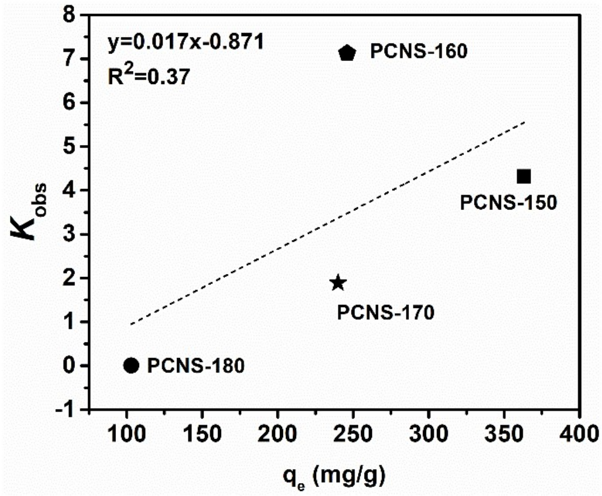

Fig. S16. Fitted curve of k_{obs} and the equilibrium adsorption capacities of BPA by PCNSs.

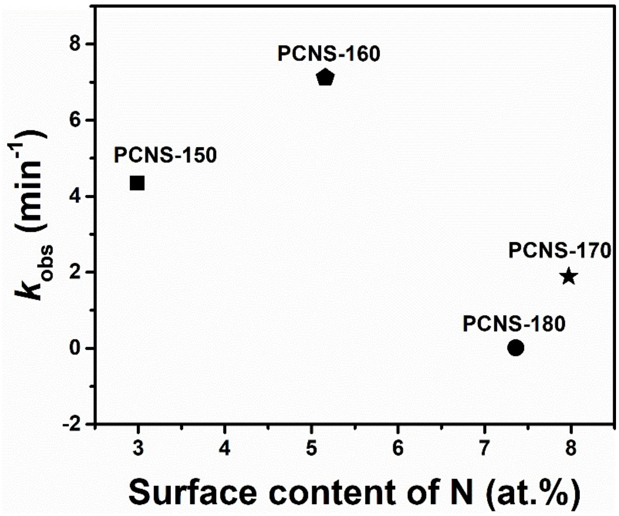

Fig. S17. Variation of k_{obs} and the surface content of N.

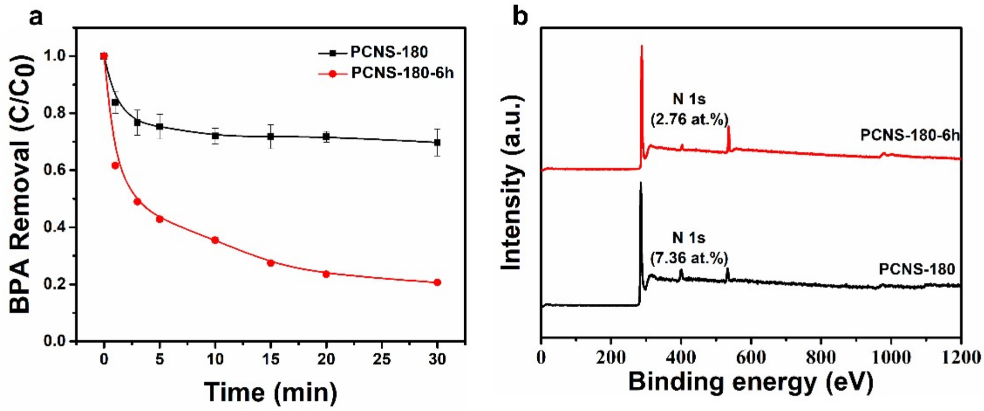

Fig. S18. (a) BPA degradation curve, (b) XPS survey of PCNS-180 and PCNS-180-6h. [PCNS] = 0.1 g/L; [PS] = 1.5 mM; [BPA] = 80 mg/L.

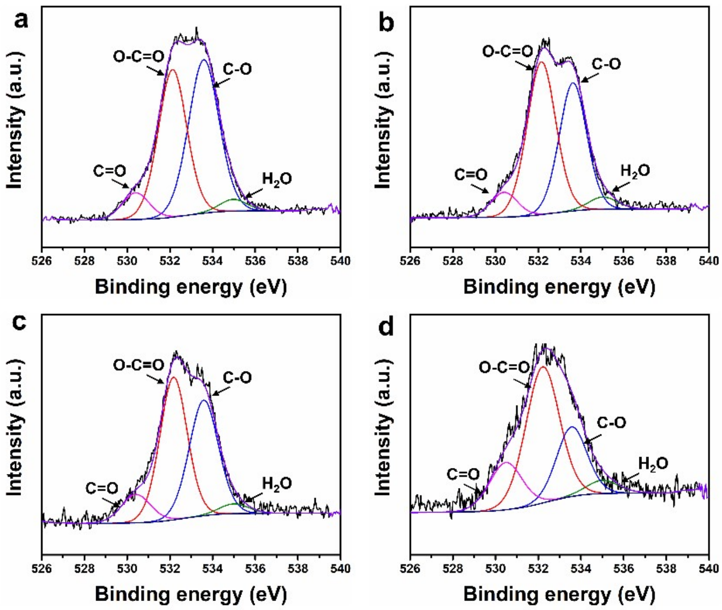

Fig. S19 High resolution XPS spectra of O 1s for (a) PCNS-150, (b) PCNS-160, (c) PCNS-170, and (d) PCNS-180.

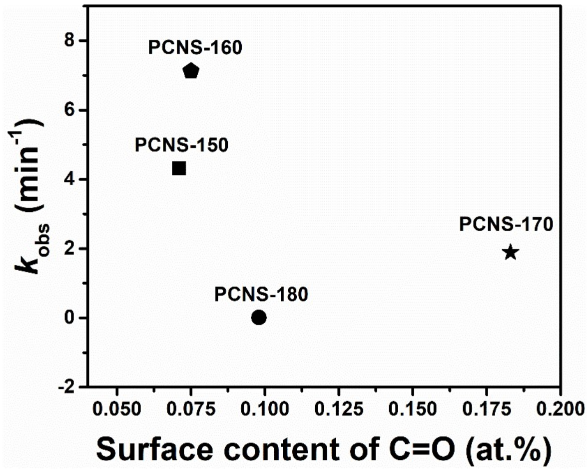

Fig. S20 Variation of k_{obs} and the surface content of C=O.

Table S1. The BET surface area, total pore volume and XPS results of all samples

Sample	S_{BET} m^2/g	total pore volume cm^3/g	XPS survey		
			C at.%	N at.%	O at.%
PCNS-150	1597	6.67	88.45	2.99	8.55
PCNS-160	1297	5.16	88.68	5.16	6.16
PCNS-170	469	1.80	89.76	7.97	2.27
PCNS-180	250	0.43	88.59	7.36	4.06

Table S2. The pseudo-first order kinetic constants (k_{obs}) of PCNS/PS system

Sample	k_{obs}	R^2
PCNS-150	4.35 min^{-1}	0.98
PCNS-160	7.12 min^{-1}	0.98
PCNS-170	1.89 min^{-1}	0.99
PCNS-180	0.01 min^{-1}	0.99

Table S3. Comparison of catalytic performances of PCNS-160 and state-of-the-art catalysts for PS or PMS activation

Study	Catalyst	Oxidant	Substrate	k_{obs} (min^{-1})
This work	PCNS-160 0.1 g/L	PS 1.5 mM	BPA 80 ppm	7.12
[1]	HCCNs 0.1 g/L	PS 1.5 mM	BPA 20 ppm	0.32
[2]	NCN-900 0.1 g/L	PS 2 mM	BPA 20 ppm	3.10
[3]	NS-2 0.1 g/L	PS 1.5 mM	BPA 20 ppm	0.18
[4]	HOPC 0.2 g/L	PS 2 mM	BPA 10 ppm	0.25
[5]	CNT 0.1 g/L	PS 2 mM	BPA 20 ppm	0.04
[6]	G-ND 0.1 g/L	PS 1.5 mM	BPA 20 ppm	0.85
[7]	SiM-1 0.4 g/L	PMS 0.27 mM	BPA 10 ppm	0.19
[8]	ZVI 0.45 g/L	PS 0.5 mM	BPA 5 ppm	0.04
[9]	Fe-Chitoal 1 g/L	PS 1 mM	BPA 10 ppm	2.11

Table S4. XPS analyses of PCNS-160 and PCNS-160-used

Sample	C at.%	N at.%	O at.%	S at.%
PCNS-160	88.68	5.16	6.16	0
PCNS-160-used	79.92	3.60	14.65	1.84

Table S5. The relative atomic percentage of various oxygen functional groups

Sample	O at.%	Fitting of the O 1s peak binding energy			
		C=O at.%	O-C=O at.%	C-O at.%	H_2O_{ads} at.%
PCNS-150	8.55	0.071	0.424	0.472	0.033
PCNS-160	6.16	0.075	0.500	0.400	0.025
PCNS-170	2.27	0.183	0.538	0.247	0.032
PCNS-180	4.06	0.098	0.467	0.402	0.033

References:

1. M. Zhang, C. Xiao, X. Yan, S. Chen, C. Wang, R. Luo, J. Qi, X. Sun, L. Wang and J. Li, Efficient removal of organic pollutants by metal-organic framework derived Co/C yolk-shell nanoreactors: Size-exclusion and confinement effect, *Environ. Sci. Technol.*, 2020, **54**, 10289−10300.
2. Y. Gao, Z. Chen, Y. Zhu, T. Li, C. Hu, New insights into the generation of singlet oxygen in the metal-free peroxymonosulfate activation process: Important role of electron-deficient carbon atoms, *Environ. Sci. Technol.*, 2020, **54**, 1232-1241.
3. Q. Yang, Y. Chen, X. Duan, S. Zhou, Y. Niu, H. Sun, L. Zhi and S. Wang, Unzipping carbon nanotubes to nanoribbons for revealing the mechanism of nonradical oxidation by carbocatalysis, *Appl. Catal. B.*, 2020, **276**, 119146.
4. C. Chu, J. Yang, D. Huang, J. Li, A. Wang, P. J. J. Alvarez and J. Kim, Cooperative pollutant adsorption and persulfate-driven oxidation on hierarchically ordered porous carbon, *Environ. Sci. Technol.*, 2019, **53**, 10352-10360
5. W. Ren, L. Xiong, X. Yuan, Z. Yu, H. Zhang, X. Duan and S. Wang, Activation of peroxydisulfate on carbon nanotubes: Electron-transfer mechanism, *Environ. Sci. Technol.*, 2019, **53**, 14595-14603.
6. H. Lee, H. I. Kim, S. Weon, W. Choi, Y. S. Hwang, J. Seo, C. Lee and J. Kim, Activation of persulfates by graphitized nanodiamonds for removal of organic compounds, *Environ. Sci. Technol.*, 2016, **50**, 10134-10142.
7. H. Song, Z. Guan, L. Chen, H. Xu, D. Xia, M. Huang and D. Li, Role of curvature in a carbon electronic structure under spatial confinement: Conversion of nonradicals to radicals, *Carbon*, 2021, **180**, 22-30.

8. L. Zhao, Y. Ji, D. Kong, J. Lu, Q. Zhou and X. Yin, Simultaneous removal of bisphenol A and phosphate in zero-valent iron activated persulfate oxidation process, *Chem. Eng. J.*, 2016, **303**, 458-466.

9. Y. G. Kang, H. C. Vu, T. T. Le, Y. S. Chang, Activation of persulfate by a novel Fe(II)-immobilized chitosan/alginate composite for bisphenol A degradation, *Chem. Eng. J.*, 2018, **353**, 736-745.